

Supporting Information

$A_x\text{Ce}_9(\text{IO}_3)_{36}$ (A = K, La): the Effect of Change for Intermediate

Valence on Second-Harmonic Generation Response

Hong-Xin Tang,^{a, b} Chao Zhuo,^b Yu-Xiao Zhang,^b Qi-Rui Shui,^b Rui-Biao Fu,^{*b} Zu-Ju Ma,^{*c} and Xin-Tao Wu^b

^a College of Chemistry and Materials Science, Fujian Normal University, Fuzhou, Fujian 350007, P. R. China

^b State Key Laboratory of Structural Chemistry, Fujian Institute of Research on the Structure of Matter, Chinese Academy of Sciences, Fuzhou, Fujian 350002, P. R. China

^c School of Materials Science and Engineering, Anhui University of Technology, Maanshan, Anhui 243002, P. R. China

*Corresponding authors, E-mails: furb@fjirsm.ac.cn; zjma@outlook.com

Experimental Procedures

1 Synthesis of $K_3Ce_9(IO_3)_{36}$ and $La_{0.3}Ce_9(IO_3)_{36}$

All chemicals were obtained commercially without further purification. In a synthetic process, single crystals were synthesized by typical hydrothermal reaction. A mixture of KIO_3 (0.4280g, 2 mmol), CeO_2 (0.0344g, 0.2 mmol) and 5mL of 0.15 mol/L H_2SO_4 was sealed in a 23 mL Teflon-lined stainless-steel autoclave. Afterward, the autoclaves were heated to 230 °C for 72 h and then cooled to 30 °C at a rate of 7 °C/h. The deep green tetrahedral crystals $K_3Ce_9(IO_3)_{36}$ were obtained in a yield of 70 % based on the Ce. Similarly, the $La_{0.3}Ce_9(IO_3)_{36}$ was synthesized by the same method except the reactants including La_2O_3 (0.0163g, 0.05 mmol), CeO_2 (0.0344g, 0.2 mmol), HIO_3 (0.7036g, 4 mmol) and 5mL of 0.15 mol/L H_2SO_4 . The yellow prism crystals were prepared in a yield of 90 % based on the Ce. These crystals were washed by distilled water several times and dried in air. The elements of K, La, Ce and I were proved by energy dispersive X-ray spectrometry (EDX) for $K_3Ce_9(IO_3)_{36}$ and $La_{0.3}Ce_9(IO_3)_{36}$, respectively (Figure S1).

2 Single Crystal X-ray Diffraction (SCXRD) Analysis

SCXRD data for $K_3Ce_9(IO_3)_{36}$ and $La_{0.3}Ce_9(IO_3)_{36}$ were collected by the Rigaku Saturn 724 CCD/AFC diffractometer with graphite-monochromated Mo $K\alpha$ radiation ($\lambda(Mo-K\alpha) = 0.71073 \text{ \AA}$). The Crystal-Clear version 1.3 program was run to reduce data. Both structures were analyzed by direct methods and used SHELXL-2014/7 to refine data by full-matrix least-squares fitting on F^2 .¹ All atoms were treated with anisotropic thermal parameters. All structural data were also checked by using the program PLATON for possible missing symmetry, and there were no higher symmetry.² Crystallographic data were summarized in Table S1. The atomic coordinates equivalent isotropic displacement parameters, selected bond lengths and angles were listed in Table S2–S7 for $K_3Ce_9(IO_3)_{36}$ and $La_{0.3}Ce_9(IO_3)_{36}$, respectively.

3 Instruments and Property Characterizations

Scanning Electron Microscopy/Energy Dispersive Analysis by X-ray (SEM/EDX)

Microprobe elemental analyses were performed on a field emission scanning electron microscope (FESEM, JSM6700F) equipped with the energy dispersive X-ray spectroscope (EDX, Oxford INCA).

Powder X-ray Diffraction (PXRD)

PXRD patterns were obtained by using graphite-monochromated Cu $K\alpha$ radiation ($\lambda = 1.540598 \text{ \AA}$) on a Rigaku Miniflex 600 diffractometer in the range of 2θ from 5 to 55° with a step size of 0.02° at room temperature.

UV–vis–NIR Diffuse Reflectance Spectroscopy

The UV–vis–NIR spectra were collected on a PrkinElmer Lambda 950 spectrophotometer with $BaSO_4$ as the reference in the wavelength range of 190–2500 nm at room temperature. The diffuse reflectance spectra were calculated into absorption spectra using the Kubelka-Munk function: $\alpha/S = F(R) = (1-R)^2/2R$, where α is the absorption coefficient, R is the reflectance, and S is the scattering coefficient, respectively.³

Infrared Spectroscopy (IR)

IR spectra were obtained on a Bruker VERTEX70 FT-IR spectrometer in 4000–400 cm^{-1} at room temperature. The dried KBr powder mixed with sample ($K_3Ce_9(IO_3)_{36}$ or $La_{0.3}Ce_9(IO_3)_{36}$) and pressed into a slice to test.

Thermogravimetric Analysis (TGA)

TGA were performed by NETZCH STA 449C instrument with 10 °C/min to heating under N₂ atmosphere from 25 to 900 °C.

Electron Paramagnetic Resonance (EPR)

EPR tests were measured by Bruker ELEXSYS E500 instrument using solid powder at room temperature.

Second-Harmonic Generation (SHG) Measurements

Powder SHG measurements were tested by Q-switch Nd: YAG laser on a modified Kurtz and Perry method in the wavelength of 1064 and 2050 nm.⁴ Because SHG intensity strongly depends on the particle size of samples, crystal samples were ground and sieved into different particle-size ranges (25–45, 45–53, 53–75, 75–109, 109–150 and 150–212 μm). KH₂PO₄ (KDP) were also ground and sieved into same particle size ranges as the relevant comparisons standard under 1064 nm laser irradiation. No index matching fluid was measured in any of the experiments.

4 Theoretical Computations

DFT calculations were performed by using the Vienna *ab initio* simulation package (VASP)⁵. The ion-electron interactions were described by the projected augmented wave (PAW)⁶ method with the valence states *2s* and *2p* for O, *5s* and *5p* for I, and *5p*, *4f*, *5d* and *6s* for Ce, respectively. The generalized gradient approximation in the Perdew-Burke-Ernzerhof (PBE) form⁷ was used. A Γ -centered 3×3×5 Monkhorst-Pack grid for the Brillouin zone sampling⁸ and a cutoff energy of 450 eV for the plane wave expansion were found to obtain convergent total energies for Ce₉(IO₃)₃₆. The simulation crystal cell includes 306 atoms with lattice parameters: *a* = *b* = 21.94 Å, and *c* = 13.26 Å, respectively. In calculation of the static $\chi^{(2)}$ coefficients, the so-called length-gauge formalism derived by Aversa and Sipe⁹ and modified by Rashkeev *et al*¹⁰ is adopted, which has been proved to be successful in calculating the second order susceptibility for semiconductors and insulators.¹¹ In the static case, the imaginary part of the static second-order optical susceptibility can be expressed as:

$$\begin{aligned} \chi^{abc} &= \frac{e^3}{\hbar^2 \Omega} \sum_{nml,k} \frac{r_{nm}^a (r_{ml}^b r_{ln}^c + r_{ml}^c r_{ln}^b)}{2\omega_{nm}\omega_{ml}\omega_{ln}} [\omega_n f_{ml} + \omega_m f_{ln} + \omega_l f_{nm}] \\ &+ \frac{ie^3}{4\hbar^2 \Omega} \sum_{nm,k} \frac{f_{nm}}{\omega_{nm}^2} [r_{nm}^a (r_{mn;c}^b + r_{mn;b}^c) + r_{nm}^b (r_{mn;c}^a + r_{mn;a}^c) + r_{nm}^c (r_{mn;b}^a + r_{mn;a}^b)] \end{aligned} \quad (1)$$

Where *r* is the position operator, $\hbar\omega_{nm} = \hbar\omega_n - \hbar\omega_m$ is the energy difference for the bands *m* and *n*, $f_{mn} = f_m - f_n$ is the difference of the Fermi distribution functions, subscripts *a*, *b*, and *c* are Cartesian indices, and $r_{mn;a}^b$ is the so-called generalized derivative of the coordinate operator in *k* space,

$$r_{mn;a}^b = \frac{r_{nm}^a \Delta_{mn}^b + r_{nm}^b \Delta_{mn}^a}{\omega_{nm}} + \frac{i}{\omega_{nm}} \times \sum_l (\omega_l r_{nl}^a r_{lm}^b - \omega_l r_{nl}^b r_{lm}^a) \quad (2)$$

where $\Delta_{nm}^a = (p_{nm}^a - p_{mm}^a) / m$ is the difference between the electronic velocities at the bands *n* and *m*. Due to the self-interaction error as well as the missing discontinuity in the stand exchange-correlation potential such as GGA and LDA,¹² the value of calculated band gap is 1.38 eV that is smaller than experimental value (2.3 eV). Thus a scissor operator has been used to correct the conduction band energy. The valence band maximum (VBM) resides between the H (-0.333 0.667 0.5) and K (-0.333 0.667 0) points in the Brillouin zone, while the conduction band minimum (CBM) lies between the G (0 0 0) and A (0 0 0.5) points (Figure 3a).

Tables

Table S1. Crystallographic data for $\text{K}_3\text{Ce}_9(\text{IO}_3)_{36}$ and $\text{La}_{0.3}\text{Ce}_9(\text{IO}_3)_{36}$

Compound	$\text{K}_3\text{Ce}_9(\text{IO}_3)_{36}$	$\text{La}_{0.3}\text{Ce}_9(\text{IO}_3)_{36}$
Formula weight	7674.78	7599.15
T (K)	293(2)	293(2)
Crystal system	trigonal	trigonal
Space group	$R\bar{3}c$	$R\bar{3}c$
a (Å)	22.1079(13)	21.9793(11)
b (Å)	22.1079(13)	21.9793(11)
c (Å)	13.2561(15)	13.0846(12)
V (Å ³)	5611.0(9)	5474.2(7)
Z	2	2
ρ_{calcd} (g·cm ⁻³)	4.543	4.610
μ (mm ⁻¹)	13.717	14.059
R_{int}	0.0519	0.0441
GOF on F^2	1.099	1.047
Flack factor	0.04(2)	-0.01(2)
R_1, wR_2 ($I > 2\sigma(I)$) ^a	0.0476, 0.1211	0.0300, 0.0749
R_1, wR_2 (all data)	0.0483, 0.1217	0.0320, 0.0757

$$^a R_1 = \sum ||F_o| - |F_c|| / \sum |F_o|; wR_2 = \{\sum w[(F_o)^2 - (F_c)^2]^2 / \sum w[(F_o)^2]^2\}^{1/2}.$$

Table S2. Atomic coordinates and equivalent isotropic displacement parameters (Å²) of $\text{K}_3\text{Ce}_9(\text{IO}_3)_{36}$.

Atom	Wyckoff	x	y	z	$U_{\text{eq}}^{[\text{a}]}$	Occ.
Ce1	18b	-0.49872(8)	-0.632(7)	-0.17032(10)	0.019(3)	1.0
I1	18b	-0.44732(8)	-0.52247(8)	-0.41001(11)	0.0194(3)	1.0
I2	18b	-0.62241(8)	-0.78445(8)	0.01804(12)	0.0195(3)	1.0
I3	18b	-0.6631(8)	-0.63374(8)	-0.04576(13)	0.0209(3)	1.0
I4	18b	-0.29355(11)	-0.48381(12)	-0.22578(17)	0.0385(5)	1.0
O1	18b	-0.5277(11)	-0.5327(12)	-0.457(20)	0.039(5)	1.0
O2	18b	-0.4236(16)	-0.5567(12)	-0.5187(18)	0.050(7)	1.0
O3	18b	-0.4823(13)	-0.6063(11)	-0.3456(14)	0.032(5)	1.0
O4	18b	-0.6614(13)	-0.6069(13)	0.0836(16)	0.037(5)	1.0
O5	18b	-0.713(11)	-0.7257(13)	-0.028(20)	0.046(6)	1.0
O6	18b	-0.5780(10)	-0.6255(10)	-0.0451(15)	0.025(4)	1.0
O7	18b	-0.5822(11)	-0.8326(11)	0.0567(20)	0.037(5)	1.0
O8	18b	-0.5685(12)	-0.7444(11)	-0.096(18)	0.039(5)	1.0
O9	18b	-0.7(11)	-0.8545(10)	-0.0463(16)	0.031(4)	1.0
O10	18b	-0.313(12)	-0.4784(15)	-0.354(20)	0.049(6)	1.0
O11	18b	-0.2381(11)	-0.5217(14)	-0.248(20)	0.047(6)	1.0
O12	18b	-0.373(13)	-0.5623(18)	-0.195(20)	0.057(8)	1.0
K1	6a	-0.3333	-0.6667	-0.1517(8)	0.0212(18)	1.0

[a] U_{eq} is defined as one-third of the trace of the orthogonalized U_{ij} tensor.

Table S3. Atomic coordinates and equivalent isotropic displacement parameters (\AA^2) of $\text{La}_{0.3}\text{Ce}_9(\text{IO}_3)_{36}$.

Atom	Wyckoff	x	y	z	$U_{\text{eq}}^{[a]}$	Occ.
Ce1	18b	0.13401(5)	0.50118(5)	0.92764(7)	0.0146(2)	1.0
I1	18b	0.03224(6)	0.36213(6)	1.13699(10)	0.0169(2)	1.0
I2	18b	0.07494(7)	0.52346(6)	0.66671(9)	0.0196(3)	1.0
I3	18b	-0.04397(6)	0.50397(6)	0.90567(9)	0.0159(2)	1.0
I4	18b	0.29581(7)	0.48655(7)	0.98094(10)	0.0264(3)	1.0
O1	18b	-0.0618(8)	0.3176(8)	1.1155(13)	0.04(4)	1.0
O2	18b	0.0414(7)	0.2849(7)	1.1352(9)	0.02(3)	1.0
O3	18b	0.0614(8)	0.3876(7)	1.0059(10)	0.026(3)	1.0
O4	18b	-0.0946(8)	0.4929(8)	1.0218(11)	0.031(3)	1.0
O5	18b	-0.0841(8)	0.4143(8)	0.8722(14)	0.036(4)	1.0
O6	18b	0.0332(7)	0.5109(8)	0.9708(12)	0.028(3)	1.0
O7	18b	0.1250(7)	0.6081(6)	0.6055(10)	0.021(3)	1.0
O8	18b	0.1356(10)	0.5568(9)	0.7766(14)	0.051(5)	1.0
O9	18b	0.0030(9)	0.5322(8)	0.7063(15)	0.049(5)	1.0
O10	18b	0.3143(7)	0.4768(8)	1.1109(12)	0.031(3)	1.0
O11	18b	0.3757(8)	0.5685(10)	0.9550(13)	0.045(4)	1.0
O12	18b	0.2383(7)	0.5225(8)	1.0035(11)	0.032(3)	1.0
La1	6a	0.3333	0.6667	0.904(3)	0.057(8)	0.1

[a] U_{eq} is defined as one-third of the trace of the orthogonalized U_{ij} tensor.

Table S4. Selected bond lengths (\AA) of $\text{K}_3\text{Ce}_9(\text{IO}_3)_{36}$.

Bond	Bond lengths	Bond	Bond lengths
Ce(1)–O(2)#1	2.36(2)	I(1)–O(3)	1.82(2)
Ce(1)–O(3)	2.38(19)	I(2)–O(7)	1.77(2)
Ce(1)–O(4)#2	2.44(2)	I(2)–O(8)	1.85(2)
Ce(1)–O(6)	2.47(18)	I(2)–O(9)	1.85(19)
Ce(1)–O(8)	2.39(2)	I(3)–O(4)	1.81(2)
Ce(1)–O(9)#3	2.41(2)	I(3)–O(5)	1.78(2)
Ce(1)–O(11)#4	2.37(2)	I(3)–O(6)	1.80(19)
Ce(1)–O(12)	2.43(3)	I(4)–O(10)	1.77(3)
I(1)–O(1)	1.79(2)	I(4)–O(11)	1.82(2)
I(1)–O(2)	1.82(2)	I(4)–O(12)	1.79(3)

#1 -1-y, -1-x, 1/2+z; #2 -2/3+y-x, -4/3-x, -1/3+z; #3 -1/3+y-x, 1/3+y, -1/6+z; #4 -1-y, -1+x-y, +z.

Table S5. Selected bond lengths (Å) of $\text{La}_{0.3}\text{Ce}_9(\text{IO}_3)_{36}$.

Bond	Bond lengths	Bond	Bond lengths
Ce(1)–O(2)#1	2.44(12)	I(1)–O(3)	1.82(14)
Ce(1)–O(3)	2.42(13)	I(2)–O(7)	1.81(12)
Ce(1)–O(4)#2	2.38(14)	I(2)–O(8)	1.85(16)
Ce(1)–O(6)	2.40(14)	I(2)–O(9)	1.76(16)
Ce(1)–O(7)#3	2.38(13)	I(3)–O(4)	1.83(13)
Ce(1)–O(8)	2.32(17)	I(3)–O(5)	1.77(15)
Ce(1)–O(11)#4	2.37(16)	I(3)–O(6)	1.83(13)
Ce(1)–O(12)	2.32(14)	I(4)–O(10)	1.79(15)
I(1)–O(1)	1.81(15)	I(4)–O(11)	1.81(17)
I(1)–O(2)	1.81(12)	I(4)–O(12)	1.82(14)

#1 $1/3-y$, $2/3+x-y$, $-1/3+z$; #2 $2/3-y$, $1/3-x$, $-1/6+z$; #3 $+x$, $1+x-y$, $1/2+z$; #4 $+y-x$, $1-x$, $+z$.

Table S6. Selected bond angles (deg.) of $\text{K}_3\text{Ce}_9(\text{IO}_3)_{36}$.

Bond	Bond angles	Bond	Bond angles
O(3)–Ce(1)–O(2)#1	137.1(9)	O(1)–I(1)–O(3)	98.4(10)
O(4)#2–Ce(1)–O(2)#1	136.8(8)	O(1)–I(1)–O(2)	98.2(14)
O(6)–Ce(1)–O(3)	132.2(7)	O(7)–I(2)–O(8)	97.3(11)
O(8)–Ce(1)–O(9)#3	147.2(8)	O(7)–I(2)–O(9)	99.5(10)
O(8)–Ce(1)–O(12)	130.8(9)	O(9)–I(2)–O(8)	97.4(10)
O(8)–Ce(1)–O(3)	126.5(8)	O(4)–I(3)–O(5)	98.7(12)
O(11)#4–Ce(1)–O(2)#1	122.0(10)	O(4)–I(3)–O(6)	96.5(10)
O(11)#4–Ce(1)–O(9)#3	137.7(8)	O(5)–I(3)–O(6)	97.8(9)
O(11)#4–Ce(1)–O(6)	139.5(7)	O(10)–I(4)–O(11)	96.7(12)
O(12)–Ce(1)–O(4)#2	144.4 (8)	O(10)–I(4)–O(12)	97.5(12)
O(12)–Ce(1)–O(6)	132.2(9)	O(11)–I(4)–O(12)	98.7(12)
O(2)–I(1)–O(3)	90.7(9)		

#1 $-1-y$, $-1-x$, $1/2+z$; #2 $-2/3+y-x$, $-4/3-x$, $-1/3+z$; #3 $-1/3+y-x$, $1/3+y$, $-1/6+z$; #4 $-1-y$, $-1+x-y$, $+z$.

Table S7. Selected bond angles (deg.) of $\text{La}_{0.3}\text{Ce}_9(\text{IO}_3)_{36}$.

Bond	Bond angles	Bond	Bond angles
O(6)–Ce(1)–O(4)#2	145.4(5)	O(1)–I(1)–O(2)	97.1(6)
O(7)#3–Ce(1)–O(2)#1	132.2(4)	O(2)–I(1)–O(3)	95.1(6)
O(7)#3–Ce(1)–O(4)#2	125.1(5)	O(4)–I(3)–O(5)	97.2(7)
O(8)–Ce(1)–O(3)	137.3(5)	O(4)–I(3)–O(6)	95.8(7)
O(8)–Ce(1)–O(7)#3	137.8(6)	O(5)–I(3)–O(6)	97.7(7)
O(11)#4–Ce(1)–O(3)	144.7(5)	O(7)–I(2)–O(8)	89.4(7)
O(11)#4–Ce(1)–O(4)#2	131.1(6)	O(7)–I(2)–O(9)	97.8(7)
O(11)#4–Ce(1)–O(2)#1	133.8(6)	O(9)–I(2)–O(8)	103.7(10)
O(12)–Ce(1)–O(2)#1	140.0(5)	O(10)–I(4)–O(11)	97.6(7)
O(12)–Ce(1)–O(6)	138.2(5)	O(10)–I(4)–O(12)	98.5(7)
O(12)–Ce(1)–O(8)	120.4(6)	O(11)–I(4)–O(12)	97.9(7)
O(1)–I(1)–O(3)	98.7(7)		

#1 $1/3-y$, $2/3+x-y$, $-1/3+z$; #2 $2/3-y$, $1/3-x$, $-1/6+z$; #3 $+x$, $1+x-y$, $1/2+z$; #4 $+y-x$, $1-x$, $+z$.

Table S8. The mass percent of K and La in $K_3Ce_9(IO_3)_{36}$ and $La_{0.3}Ce_9(IO_3)_{36}$, respectively.

Element	Calculated (%)	EDX (%)
K [$K_3Ce_9(IO_3)_{36}$]	1.53	1.73
La [$La_{0.3}Ce_9(IO_3)_{36}$]	0.55	0.36

Table S9. Calculation of dipole moment (*c*-component) of BBUs (IO_3 and CeO_8 units) and net dipole moment for a unit cell and the dipole moment per unit volume in $K_3Ce_9(IO_3)_{36}$ and $La_{0.3}Ce_9(IO_3)_{36}$.

Compound	BBUs	Dipole moment (D) <i>c</i> -component	Net dipole moment (D) (a unit cell)	Dipole moment per unit volume (D Å ⁻³)
$K_3Ce_9(IO_3)_{36}$	I(1)O ₃	-6.66	-238.68	-0.043
	I(2)O ₃	-7.99		
	I(3)O ₃	11.02		
	I(4)O ₃	-9.63		
	Ce(1)O ₈	3.17	57.06	0.01
$La_{0.3}Ce_9(IO_3)_{36}$	I(1)O ₃	-10.7	253.26	0.046
	I(2)O ₃	5.53		
	I(3)O ₃	9.69		
	I(4)O ₃	9.55		
	Ce(1)O ₈	-3.39	-61.02	-0.01

Figures

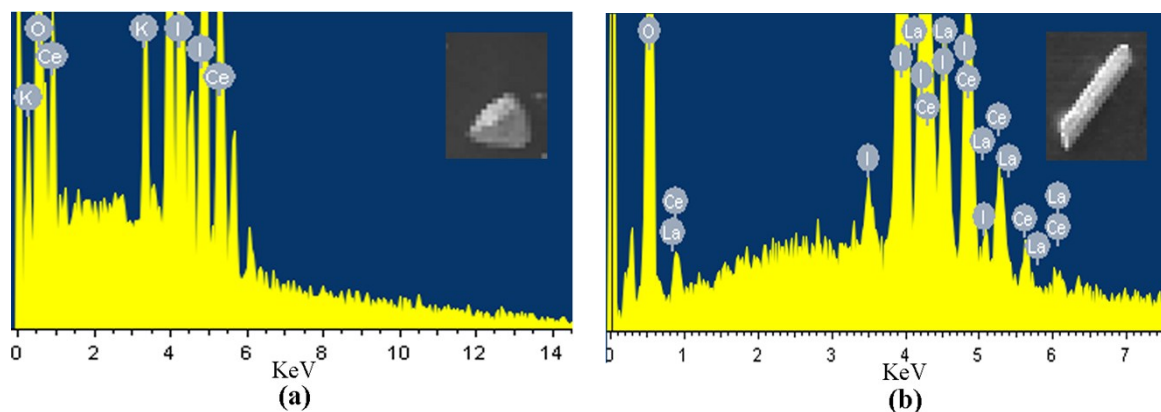


Figure S1. EDX spectra of (a) $K_3Ce_9(IO_3)_{36}$ and (b) $La_{0.3}Ce_9(IO_3)_{36}$

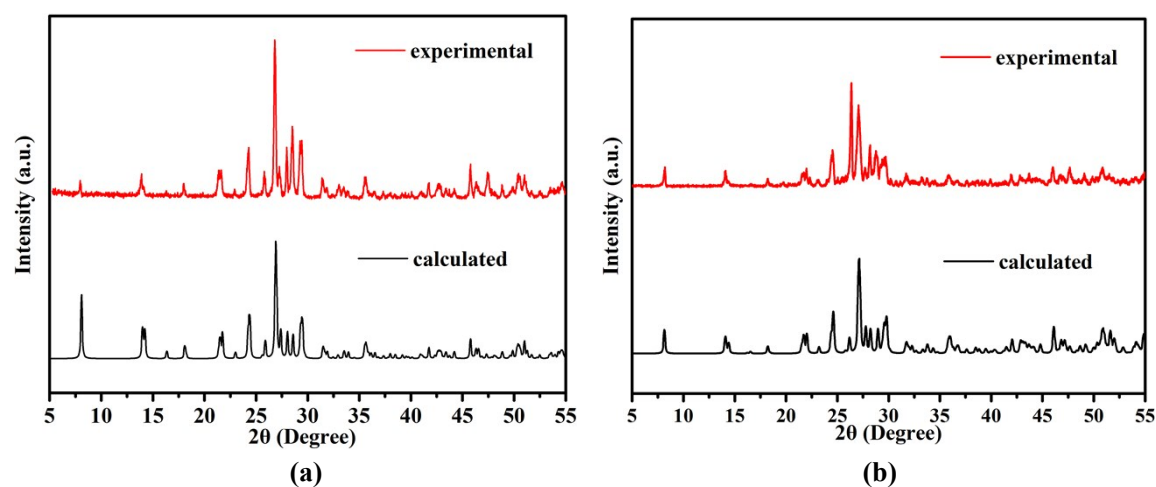


Figure S2. PXRD patterns of (a) $K_3Ce_9(IO_3)_{36}$ and (b) $La_{0.3}Ce_9(IO_3)_{36}$

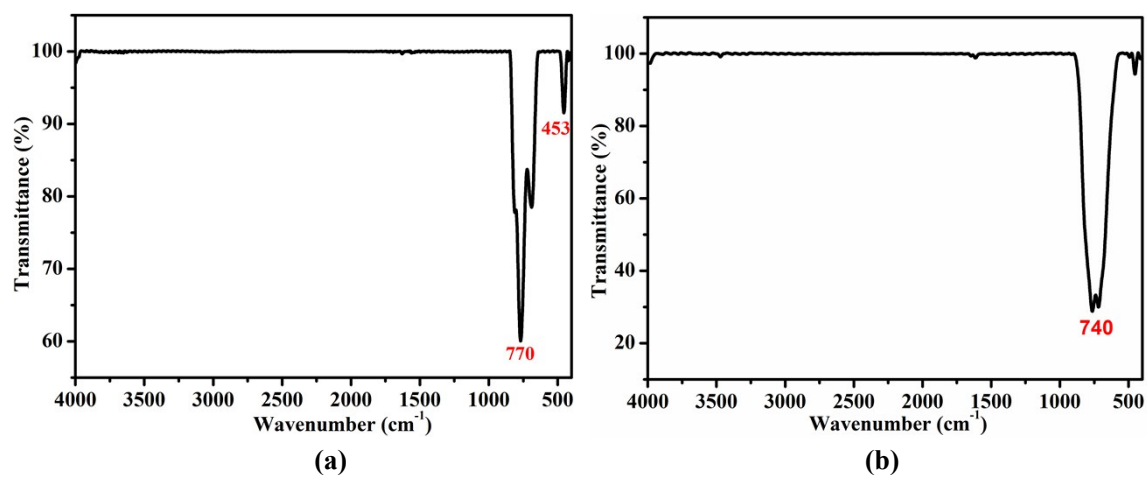


Figure S3 IR spectra of (a) $K_3Ce_9(IO_3)_{36}$ and (b) $La_{0.3}Ce_9(IO_3)_{36}$

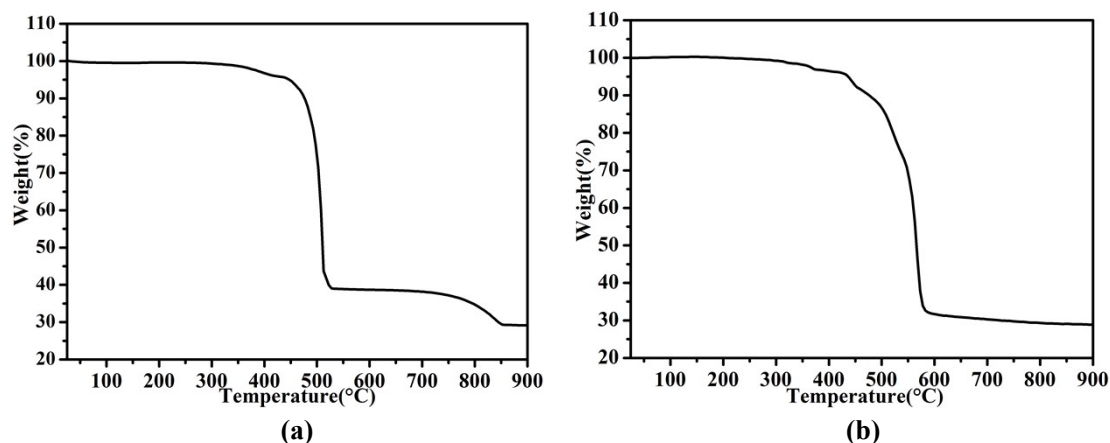


Figure S4. TG curves of (a) $\text{K}_3\text{Ce}_9(\text{IO}_3)_{36}$ and (b) $\text{La}_{0.3}\text{Ce}_9(\text{IO}_3)_{36}$

References

- 1 G. M. Sheldrick, *Acta Crystallographica Section C: Structural Chemistry*, 2015, 71, 3-8.
- 2 A. Spek, *J. Appl. Crystallogr.*, 2003, 36, 7-13.
- 3 (a) P. Kubelka and F. Munk, *Z. Tech. Phys.*, 1931, 12;(b) J. Tauc, *Mater. Res. Bull.*, 1970, 5, 721-729.
- 4 S. K. Kurtz and T. T. Perry, *J. Appl. Phys.*, 1968, 39, 3798-3813.
- 5 (a) G. Kresse and J. Furthmuller, *Phys. Rev. B: Condens. Matter*, 1996, 54, 11169-11186;(b) G. Kresse and D. Joubert, *Phys. Rev. B: Condens. Matter*, 1999, 59, 1758-1775.
- 6 P. E. Blochl, *Phys. Rev. B: Condens. Matter*, 1994, 50, 17953-17979.
- 7 J. P. Perdew, K. Burke and M. Ernzerhof, *Phys Rev Lett*, 1996, 77, 3865-3868.
- 8 H. J. Monkhorst and J. D. Pack, *Phys. Rev. B: Condens. Matter*, 1976, 13, 5188.
- 9 C. Aversa and J. E. Sipe, *Phys Rev B*, 1995, 52, 14636-14645.
- 10 (a) S. N. Rashkeev, W. R. L. Lambrecht and B. Segall, *Phys Rev B*, 1998, 57, 3905;(b) S. N. Rashkeev, W. R. Lambrecht and B. Segall, *Phys. Rev. B*, 1998, 57, 3905.
- 11 (a) J. Hu, Z. Ma, J. Li, C. He, Q. Li and K. Wu, *J Phys D Appl Phys*, 2016, 49, 85103-85103;(b) J. Li, Z. Ma, C. He, Q. Li and K. Wu, *J Mater Chem C*, 2016, 4, 1926-1934;(c) Z. Ma, K. Wu, R. Sa, K. Ding and Q. Li, *Aip Advances*, 2012, 2, 032170;(d) Z. Ma, K. Wu, R. Sa, Q. Li and Y. Zhang, *J. Alloys Compd.*, 2013, 568, 16-20.
- 12 (a) S. Lany and A. Zunger, *Phys Rev B*, 2010, 81;(b) N. Umezawa, O. Y. Shuxin and J. H. Ye, *Phys Rev B*, 2011, 83, 035202.